Optimized Series Dynamic Braking Resistor for LVRT of Doubly-Fed Induction Generator With Uncertain Fault Scenarios

JIEJIE HUANG[ID]1, **LEI ZHANG**[ID]1, **(Member, IEEE), SHUN SANG**[ID]1, **XIAOCEN XUE**1, **XINSONG ZHANG**1, **TINGTING SUN**[ID]2, **WEIMIN WU**[ID]3, **(Member, IEEE), AND NING GAO**[ID]3, **(Associate Member, IEEE)**

[1]School of Electrical Engineering, Nantong University, Nantong 226019, China
[2]School of Electrical and Energy Engineering, Nantong Institute of Technology, Nantong 226002, China
[3]Department of Electrical Engineering, Shanghai Maritime University, Shanghai 201306, China

Corresponding author: Lei Zhang (nttzzl@ntu.edu.cn)

ABSTRACT The terminal-connected series dynamic braking resistor (SDBR) is applied to assist the low-voltage ride-through (LVRT) of the doubly-fed induction generator (DFIG). With the fault current and switch-in of the SDBR, the stator voltage oscillates, thus the constant stator voltage drop assumption is invalid and the effect of the converter current control is weakened with the changing voltage-oriented reference frame. In this paper, the xy frame of the point of common coupling is applied to the converter control to avoid oscillation of the reference frame. The analytical expression of fault current with the SDBR and constant converter current control is derived. To evaluate the LVRT effect, the analytical analysis of the LVRT transient is carried out. The resistance of the SDBR is optimized based on an index combining the capabilities of the DFIG to provide the active power support and damp the electromagnetic torque oscillation. The uncertainties of the fault scenario are considered in the optimization algorithm by applying the probabilistic method. Simulation results show that the improved LVRT effect of the DFIG is realized with optimization to the SDBR resistance and its switch-in criterion.

INDEX TERMS Doubly-fed induction generator, low-voltage ride-through, series dynamic braking resistor, constant current control, analytical fault current expression, fault uncertainties, probabilistic evaluation.

I. INTRODUCTION

With the integration of wind power generation, the stability issues of wind power system have attracted much attention and are extensively studied in the existing literatures [1]–[3]. A major concern for the wind turbine generator is low-voltage ride-through (LVRT) capability [4], which is included in the requirements of the grid codes for the wind power integration. The series dynamic braking resistor (SDBR) may be applied as the hardware protection scheme to assist the LVRT of the doubly-fed induction generator (DFIG) [5]–[7]. The advantages of the SDBR include low cost and easy implementation.

The associate editor coordinating the review of this manuscript and approving it for publication was Jamshid Aghaei[ID].

To assist the LVRT of the DFIG, the SDBR may be placed at different locations, e.g., at the stator side, at the rotor side, or at the generator terminal. The SDBR helps to reduce the electromagnetic torque oscillation of the DFIG during LVRT, but its overall capability to assist the LVRT is affected by its position. In [8]–[11] and [12], the SDBR is separately placed at the stator side and the rotor side of the DFIG as the passive LVRT compensator. Its effect to suppress the rotor current is analyzed through analytical analysis of the LVRT transient in [13]. Ref [14] compares the LVRT effects between SDBR at the stator side and at the rotor side, and concludes that the stator-side SDBR has advantages in the aspects of increasing the stator voltage, reducing DC component of the transient stator flux, and improve damping to electromagnetic torque oscillation. The comprehensive research on the LVRT effect

of the SDBR with the different implementation positions is carried out in [15], which draws the following conclusion that, for the SDBR placed at the terminal, not only the stator voltage is increased, voltage of the grid-side converter (GSC) is also raised. This helps to enhance the capability of the GSC to output power during the LVRT. The increased active power output helps to maintain the power balance between the rotor-side converter (RSC) and the GSC for the DC-link voltage control. While the increased reactive power output helps to support the grid voltage. Related research reveals that, placing the SDBR at the generator terminal is the most effective method to assist the LVRT of the DFIG. Although this scheme has seen wide application, improvement in the following three aspects is still needed to further enhance its capability to assist the LVRT, which are motivations of the research in this paper.

(i) Coordination between SDBR and converter control in aspects of vector control reference frame and reactive current injection capability

With the SDBR to damp the electromagnetic oscillation of the DFIG and limit the peak fault current during the LVRT, the current control by the converter may be retained. To assist LVRT of the DFIG, control strategies of the converters are developed with the SDBR placed at the stator side [8] and at the rotor side [12], which are referred to as active LVRT schemes. Coordination between the SDBR and the converter control is required to enhance the LVRT effect. In [16], to avoid slow response during the LVRT, the outer-loop power control of the converter is replaced by the constant current control to achieve fast transition to desired operation status of the DFIG. The current control of the converter needs to be adjusted with the switch-in of the SDBR. Rahimi *et al* in [8] consider the increased stator resistance by the SDBR when determining the current reference of the RSC. Given that the resistance of the SDBR is fixed, its capability to compensate for the stator voltage drop during the LVRT relies on flexible adjustment to the current reference of converter. The above research shows that it is necessary to coordinate the SDBR and the converter control during the LVRT.

What has not been considered in the coordination between the SDBR and the converter control is the reference frame of the converter control with the switched-in SDBR. When the voltage drop occurs at the terminal, SDBR switches in for the LVRT. With the oscillating fault current flowing through the SDBR, phase angle difference between the terminal voltage and the stator voltage oscillates. Normally, the vector control of the converter current is realized in the dq reference frame with the stator voltage vector aligned to the direct axis. With oscillating phase angle difference between the dq reference frame and the xy reference frame (corresponding to voltage at the point of common coupling (PCC)), the constant current control of the converter in dq reference frame is transformed into oscillating current in xy reference frame, indicating that the effect of the constant current control is weakened when it comes to controlling the fault current injected to the grid during the LVRT.

As for existing studies on the terminal-placed SDBR, such as [17], its impact on the reference frame of converter control has not yet been analyzed. To realize effective control over the converter current, a modified vector control scheme for the converter needs to be established.

The SDBR scheme lacks the capability to inject reactive current to the grid during the LVRT which is required by the grid codes, as pointed out in [18]. Additional equipment such as the STATCOM is applied to enhance the reactive current support capability in [19]. However, this increases the system cost due to the extra investment. The preferred solution is to fully utilize the reactive power capacity of the converters to inject the required reactive current. The existing studies have tried to separately use the RSC [20] and the GSC [21] for the reactive current support. These schemes are likely to cause violations to current constraints of the converters under deep voltage dips, as the required reactive current is proportional to the voltage drop depth. It helps to enhance the reactive current support capability of the DFIG by coordinating the RSC and the GSC to jointly output the reactive current when the SDBR switches in. The desirable LVRT effect may be ensured by determining the current references based on pre-evaluation of their LVRT effects instead of directly assigning them according to the grid code as [22] does.

(ii) Analytical LVRT analysis of the DFIG with terminal-connected SDBR

For the evaluation of the LVRT effect, analytical analysis is needed to quantify the parameters of the DFIG during the LVRT. In the existing studies, analytical analysis is carried out by prescribing the fixed voltage drop to the terminal of the DFIG, which is normally approximated to voltage drop at the stator side. For example, Ref [23] solves the analytical fault current expression of the DFIG by directly prescribing the stator voltage drop.

However, with the terminal-connected SDBR in operation, the stator voltage varies both in magnitude and phase angle as the oscillating fault current flowing through it during the LVRT. With terminal-connected SDBR, existing analytical LVRT analysis needs to be updated, as traditional methods solve the fault current expression with fixed voltage drop of the stator. While in this case, fault current is not only affected by the stator voltage, fault current oscillation also has reverse impact on the stator voltage. Since the fault current flowing through SDBR includes both the stator and the GSC current, the GSC current also needs to be included in the fault current model, which adds difficulty to the analytical LVRT analysis.

(iii) Optimization of SDBR resistance to improve overall LVRT effect with uncertain fault scenarios

With the fixed resistance of the SDBR, its value needs to be carefully chosen to guarantee the desirable LVRT effect. The existing studies mainly focus on the operational security of the DFIG, i.e., the feasible range of the SDBR resistance are decided based on safety constraints of the DFIG. Soliman *et al* determine the feasible range of the SDBR resistance at the stator side considering the voltage constraints of the stator and the RSC in [11]. Similar research

is done with the SDBR at the rotor side with the constraints of the rotor current and RSC voltage considered, as referred in [13]. They both adopt fault current expression derived based on prescribed voltage drop at the stator side. Thus, they may not be applied to the changing stator voltage with the terminal-connected SDBR.

The existing analytical analysis is mainly applied to check security constraints instead of quantifying the LVRT effect. When selecting the SDBR resistance for the improved LVRT effect, Refs [10] and [24] compare time-domain simulation results to obtain the optimal SDBR resistance. This method lacks the quantitive index to evaluate LVRT effect, making it difficult to formulate the optimization model. Besides, time-domain simulation requires more calculations compared with the analytical analysis, making it the less efficient method to optimize the SDBR resistance.

To further select the SDBR resistance within its feasible range for the optimal LVRT effect, optimization model based on analytical LVRT analysis needs to be established so as to determine optimal SDBR resistance with clear optimization target, i.e., the comprehensive index to quantify the overall LVRT effect. This index is not supposed to solely focus on one single aspect of the LVRT performance. For example, if this index only quantifies capability of the SDBR to suppress the fault current oscillation, then the optimization model of the SDBR yields high resistance value to enhance damping to electromagnetic oscillations. However, with the high SDBR resistance applied to the DFIG terminal, the feasible range of the output current is reduced considering the stator voltage constraint, which limits the capability of the DFIG to provide frequency and voltage support to the integrated grid during the LVRT. Thus, the comprehensive index of the LVRT is needed for the optimization model.

Another thing that is ignored in the selection of the SDBR resistance is the uncertainty of the fault scenarios. The fixed SDBR resistance provides varied LVRT performances under different fault scenarios. For example, when the large SDBR resistance that may compensate for the deep voltage drops is applied to minor voltage drops, the active and reactive output current of the DFIG is limited due to stator voltage constraint. The comparison of the LVRT effects with the SDBR under different fault scenarios has been made in the existing works, with the DFIG [25], the squirrel cage induction generator [26], and the permanent magnet synchronous generator [27] respectively. Still, the method to determine a compromised SDBR resistance value with satisfactory LVRT effect both under deep voltage drops and minor voltage drops has not yet been studied. To optimize the SDBR resistance considering varied fault scenarios, the uncertainty of the fault scenarios needs to be considered when evaluating the LVRT effect of the SDBR. In [28], the uncertainty of the fault scenario is described based on the probability distribution. To improve the overall LVRT effect under different fault scenarios, the method to determine the SDBR resistance that achieves the probabilistic optimal LVRT effect needs to be developed.

In this paper, the terminal-connected SDBR is applied for the LVRT of the DFIG. Impact of the SDBR on the converter control is considered. The xy frame of the PCC is adopted to avoid oscillation of the reference frame. The analytical fault current expression of the DFIG with the SDBR is derived. An index combining the capabilities of supporting the active power and damping the electromagnetic torque oscillation is adopted to evaluate the LVRT effect of the DFIG, based on which optimal SDBR resistance under given fault condition is determined. The influence of the uncertainties of the fault scenario, e.g., the wind speed, voltage drop depth, and fault duration on the selection of the SDBR resistance is analyzed. Based on the probability distribution of the fault uncertainties and corresponding LVRT effects, expectation of the LVRT effect index is calculated to evaluate the overall LVRT effect, which is applied to optimize both the SDBR resistance and the switch-in criterion for the optimal overall LVRT effect. The influence of the switch-in criterion of the SDBR and the corresponding LVRT effect are discussed. Numerical results validate the accuracy of the analytical LVRT analysis and the effectiveness of the proposed SDBR scheme to improve the LVRT effect of the DFIG.

This paper is organized as follows. Section II analyses the LVRT transient of the DFIG with terminal-connected SDBR using the analytical method. The impact of the SDBR on the converter control is analyzed and the new reference frame is adopted for the converter control. The voltages of the RSC and GSC are quantified. In Section III, optimization model to SDBR resistance for the optimal LVRT effect is established based on the analytical analysis carried out in Section II. The uncertainties of fault scenarios are considered to determine the SDBR resistance. The effectiveness and accuracy of the proposed model are validated by numerical results in Section IV. The yielded conclusions are given in Section V.

II. ANALYTICAL ANALYSIS ON LVRT TRANSIENT OF DFIG WITH TERMINAL-CONNECTED SDBR
A. ANALYTICAL EXPRESSION OF DFIG FAULT CURRENT
The configuration of the DFIG with the terminal-connected SDBR is shown in Fig. 1, where V, I, R and Z are the voltage, current, resistance and impedance, respectively. Subscripts s, r, g, ST denote stator, RSC, GSC, and step-up transformer, respectively. The SDBR is bypassed during normal operation. Once the voltage drop at the PCC is detected, the SDBR is switched in to raise the terminal voltage of the DFIG, damp the electromagnetic torque oscillation, and avoid over speed of the rotor caused by the decreased active power output. The DC-chopper circuit is applied to avoid the overvoltage of DC bus caused by power imbalance between RSC and GSC.

Under motor convention, flux and voltage equations of the DFIG in the synchronous reference frame are given by (1).

$$\begin{cases} \boldsymbol{V}_s = R_s \boldsymbol{I}_s + j\omega_0 \boldsymbol{\psi}_s + p\boldsymbol{\psi}_s \\ \boldsymbol{V}_r = R_r \boldsymbol{I}_r + js\omega_0 \boldsymbol{\psi}_r + p\boldsymbol{\psi}_r \\ \boldsymbol{\psi}_s = L_s \boldsymbol{I}_s + L_m \boldsymbol{I}_r \\ \boldsymbol{\psi}_r = L_r \boldsymbol{I}_r + L_m \boldsymbol{I}_s \end{cases} \tag{1}$$
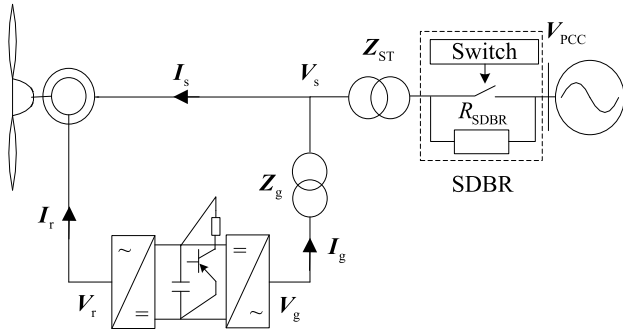
FIGURE 1. Configuration of DFIG with terminal-connected SDBR.

where L is the inductance, L_m is the mutual inductance, ω_0 is the synchronous speed, p is the differential operator, ψ is the flux, s is the slip.

After the switch-in of the SDBR, the voltage equation of the PCC is written as,

$$V_{PCC} = V_s + (I_s - I_g)(R_{ST} + R_{SDBR} + j\omega_0 L_{ST}) \quad (2)$$

By combining (1) and (2), a 1st order differential equation of the stator flux is obtained, as given by,

$$
\begin{aligned}
&p\psi_s + \left(\frac{R_s + R_{ST} + R_{SDBR} + j\omega_0 L_{ST}}{L_s} + j\omega_0 \right) \psi_s \\
&= V_{PCC} + \left(I_g + \frac{L_m I_r}{L_s} \right) \\
&\quad \times (R_{ST} + R_{SDBR} + j\omega_0 L_{ST}) + \frac{L_m R_s}{L_s} I_r \quad (3)
\end{aligned}
$$

The analytical expression of the stator flux is derived by solving the differential equation (3). During the LVRT, the dual-loop PI control of the RSC is replaced by direct inner-loop current control to realize fast response during the LVRT. Thus, it is assumed that the RSC and GSC current quickly reaches the reference. In this case, the converter current is approximated to its reference value to solve (3). The derived expression of the stator flux (4) indicates that it follows the exponential decay. The detailed parameters are given in (5).

$$\psi_s = \psi_s^{\infty} + \left(\psi_s^{\infty} - \psi_s^{ini} \right) e^{-\tau t} \quad (4)$$

$$
\begin{cases}
Z_{ST} = R_{ST} + j\omega_0 L_{ST} \\
\psi_s^{ini} = \left(V_{PCC}^{ini} - R_s I_s^{ini} - \left(I_s^{ini} - I_g^{ini} \right) Z_{ST} \right) / j\omega_0 \\
\psi_s^{\infty} = \dfrac{\sigma V_{PCC}^{ini} + \left(I_g^{ref} + \frac{L_m I_r^{ref}}{L_s} \right)(Z_{ST} + R_{SDBR}) + \frac{L_m R_s}{L_s} I_r^{ref}}{\frac{R_s + R_{SDBR} + Z_{ST}}{L_s} + j\omega_0} \\
\tau = \dfrac{R_s + R_{SDBR} + Z_{ST}}{L_s} + j\omega_0
\end{cases} \quad (5)
$$

where σ is the voltage drop depth of PCC, τ is the damping time constant, and superscript ini denotes initial state value, ∞ denotes steady state value.

Based on the stator flux expression, the stator current and the total fault current of the DFIG are obtained, as given by,

$$
\begin{cases}
I_s = \dfrac{\psi_s - L_m I_r^{ref}}{L_s} \\
I_f = I_s + I_g^{ref}
\end{cases} \quad (6)
$$

where I_f is the total fault current of the DFIG.

B. MODIFICATION TO REFERENCE FRAME OF CONVERTER CONTROL

Equation (3) needs to be solved within the same reference frame. Normally, the vector control of the converter current is realized in the dq frame with stator voltage aligned to the direct axis, i.e., d-axis. Meanwhile, PCC voltage is aligned to the x-axis of the xy frame adopted by the integrated power system. Thus, analytical calculation involves the coordinate transformation between the dq frame and the xy frame.

In Fig. 2, relationship between the PCC voltage vector and the stator voltage vector is illustrated to show the phase angle difference between the two reference frames. Equations (4)-(6) reveal that the stator current follows exponential decay as the stator flux does. It is shown in Fig. 2 that, as the stator current rotates from $(\psi_s^{ini} - L_m I_r^{ref})/L_s$ to $(\psi_s^{\infty} - L_m I_r^{ref})/L_s$, at angular speed $(L_{ST}/L_s + 1)\omega_0$ in anti-clockwise direction, the phase angle difference between dq frame and xy frame varies before the stator current reaches the steady state.
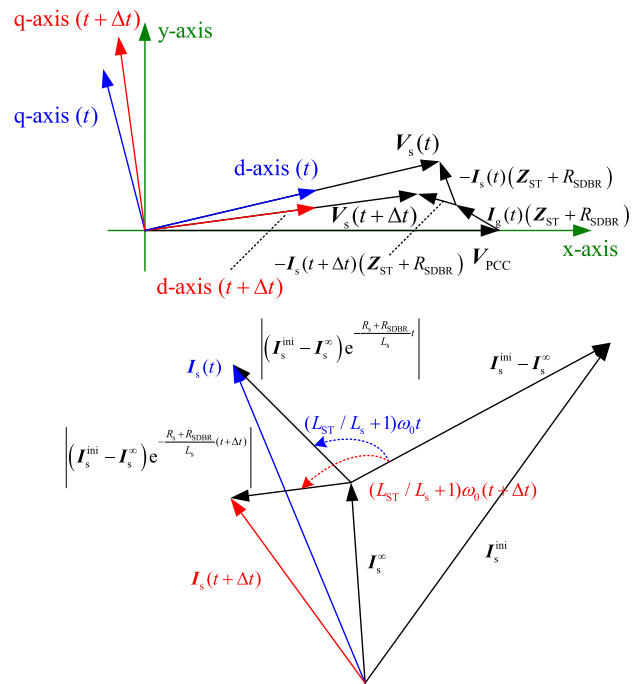

FIGURE 2. Variation of phase angle difference between dq frame and xy frame during stator current oscillation.

At this stage, controlled constant currents of the converters in the dq frame will be transformed into oscillating currents

in the xy frame, leading to the oscillation of the steady-state stator flux and the prolonged stabilization process. To solve the problem, the current control to the converter is realized in the xy frame instead of the traditional dq frame.

C. ANALYTICAL ANALYSIS ON CONTROL INPUT AND EFFECT OF CURRENT CONTROL BY CONVERTERS

During the LVRT, the outer-loop power control of converters is abandoned due to its slow response. To provide the desired power output of the stator and GSC, corresponding current references are decided by solving the equation set (7), which are then applied to the direct inner-loop current control.

$$
\begin{cases}
\boldsymbol{I}_s^\infty = \left(\boldsymbol{\psi}_s^\infty - L_m \boldsymbol{I}_r^{\text{ref}} \right)/L_s \\
\boldsymbol{V}_s^\infty = \sigma \boldsymbol{V}_{\text{PCC}}^{\text{ini}} + \left(\boldsymbol{I}_g^{\text{ref}} - \boldsymbol{I}_s^\infty \right)(\boldsymbol{Z}_{\text{ST}} + R_{\text{SDBR}}) \\
P_s^{\text{ref}} = -\text{Re}\left[\boldsymbol{V}_s^\infty \left(\boldsymbol{I}_s^\infty \right)^* \right] \\
Q_s^{\text{ref}} = -\text{Im}\left[\boldsymbol{V}_s^\infty \left(\boldsymbol{I}_s^\infty \right)^* \right] \\
P_g^{\text{ref}} = \text{Re}\left[\boldsymbol{V}_s^\infty \left(\boldsymbol{I}_g^{\text{ref}} \right)^* \right] \\
Q_g^{\text{ref}} = \text{Im}\left[\boldsymbol{V}_s^\infty \left(\boldsymbol{I}_g^{\text{ref}} \right)^* \right]
\end{cases}
\tag{7}
$$

where P and Q are active and reactive power, and superscript $*$ denotes conjugate.

Through derivation based on (1), voltage equations of the RSC and the GSC are rewritten as (8) and (9) respectively.

$$
\boldsymbol{V}_r = R_r \boldsymbol{I}_r + L_r' p \boldsymbol{I}_r + j s \omega_0 L_r' \boldsymbol{I}_r
$$
$$
- j \frac{L_m}{L_s}(1-s)\,\omega_0 \left(L_s \boldsymbol{I}_s + L_m \boldsymbol{I}_r \right) + \frac{L_m}{L_s}\left(\boldsymbol{V}_s - R_s \boldsymbol{I}_s \right)
\tag{8}
$$

$$
\boldsymbol{V}_g = R_g \boldsymbol{I}_g + L_g \frac{d\boldsymbol{I}_g}{dt} + j \omega_0 L_g \boldsymbol{I}_g + \boldsymbol{V}_s
\tag{9}
$$

The PI control is applied to adjust voltages of the RSC and the GSC to output the desired converter current. The control equations of the RSC and the GSC are given by (10) and (11) respectively. The stator flux oscillation yielded by voltage drop is added as the feed-forward compensation term in the RSC control to prevent its impact on the rotor current [29].

$$
\boldsymbol{V}_r = k_{\text{pr}}\left(\boldsymbol{I}_r^{\text{ref}} - \boldsymbol{I}_r \right) + k_{\text{ir}} \int \left(\boldsymbol{I}_r^{\text{ref}} - \boldsymbol{I}_r \right) dt + j s \omega_0 L_r' \boldsymbol{I}_r
$$
$$
- j \frac{L_m}{L_s}(1-s)\,\omega_0 \left(L_s \boldsymbol{I}_s + L_m \boldsymbol{I}_r \right)
$$
$$
+ \frac{L_m}{L_s}\left(\boldsymbol{V}_s - R_s \boldsymbol{I}_s \right)
\tag{10}
$$

$$
\boldsymbol{V}_g = k_{\text{pg}}\left(\boldsymbol{I}_g^{\text{ref}} - \boldsymbol{I}_g \right) + k_{\text{ig}} \int \left(\boldsymbol{I}_g^{\text{ref}} - \boldsymbol{I}_g \right) dt
$$
$$
+ j \omega_0 L_g \boldsymbol{I}_g + \boldsymbol{V}_s
\tag{11}
$$

where $L_r' = L_r - L_m^2/L_s$, k_{pr}, k_{ir}, k_{pg} and k_{ig} denote proportional coefficients and integral coefficients of the RSC and GSC. Superscript ref denotes the reference value.

The converter control is analyzed in the aspects of control input and effect, i.e., voltage and current of RSC and GSC.

The control equations of the RSC and GSC are separately combined with their voltage equations to solve the converter current. By combining (8) and (10), the 2$^{\text{nd}}$ order differential equation of the RSC current is obtained, as given by,

$$
\frac{d^2 \boldsymbol{I}_r}{dt^2} + \frac{\left(R_r + k_{\text{pr}} \right) \omega_0}{L_r'} \frac{d\boldsymbol{I}_r}{dt} + \frac{k_{\text{ir}} \omega_0^2}{L_r'} \boldsymbol{I}_r = \frac{k_{\text{ir}} \omega_0^2}{L_r'} \boldsymbol{I}_r^{\text{ref}}
\tag{12}
$$

Solving (12), the RSC current is given by,

$$
\boldsymbol{I}_r = \boldsymbol{I}_r^{\text{ref}} + c_1 e^{r_1 t} + c_2 e^{r_2 t}
\tag{13}
$$

Coefficients r_1, r_2, c_1 and c_2 are given by,

$$
\begin{cases}
r_{1,2} = -\dfrac{\left(R_r + k_{\text{pr}} \right) \omega_0}{2L_r'} \\
\qquad \pm \dfrac{1}{2}\sqrt{\left[\dfrac{\left(R_r + k_{\text{pr}} \right) \omega_0}{L_r'} \right]^2 - 4\dfrac{k_{\text{ir}}\omega_0^2}{L_r'}} \\
c_1 = \dfrac{p\boldsymbol{I}_r^{\text{ini}} - r_2 \left(\boldsymbol{I}_r^{\text{ini}} - \boldsymbol{I}_r^{\text{ref}} \right)}{r_1 - r_2} \\
c_2 = \dfrac{p\boldsymbol{I}_r^{\text{ini}} - r_1 \left(\boldsymbol{I}_r^{\text{ini}} - \boldsymbol{I}_r^{\text{ref}} \right)}{r_2 - r_1} \\
p\boldsymbol{I}_r^{\text{ini}} = \omega_0 k_{\text{pr}} \left(\boldsymbol{I}_r^{\text{ref}} - \boldsymbol{I}_r^{\text{ini}} \right)/L_r'
\end{cases}
\tag{14}
$$

Combining (9) and (11), the 2$^{\text{nd}}$ order differential equation of the GSC current is given by,

$$
\frac{d^2 \boldsymbol{I}_g}{dt^2} + \frac{\left(R_g + k_{\text{pg}} \right) \omega_0}{L_g} \frac{d\boldsymbol{I}_g}{dt} + \frac{k_{\text{ig}} \omega_0^2}{L_g} \boldsymbol{I}_g = \frac{k_{\text{ig}} \omega_0^2}{L_g} \boldsymbol{I}_g^{\text{ref}}
\tag{15}
$$

Solving (15), the GSC current is given by,

$$
\boldsymbol{I}_g = \boldsymbol{I}_g^{\text{ref}} + c_3 e^{r_3 t} + c_4 e^{r_4 t}
\tag{16}
$$

Coefficients r_3, r_4, c_3 and c_4 are given by,

$$
\begin{cases}
r_{3,4} = -\dfrac{\left(R_g + k_{\text{pg}} \right) \omega_0}{2L_g} \\
\qquad \pm \dfrac{1}{2}\sqrt{\left[\dfrac{\left(R_g + k_{\text{pg}} \right) \omega_0}{L_g} \right]^2 - 4\dfrac{k_{\text{ig}}\omega_0^2}{L_g}} \\
c_3 = \dfrac{p\boldsymbol{I}_g^{\text{ini}} - r_4 \left(\boldsymbol{I}_g^{\text{ini}} - \boldsymbol{I}_g^{\text{ref}} \right)}{r_3 - r_4} \\
c_4 = \dfrac{p\boldsymbol{I}_g^{\text{ini}} - r_3 \left(\boldsymbol{I}_g^{\text{ini}} - \boldsymbol{I}_g^{\text{ref}} \right)}{r_4 - r_3} \\
p\boldsymbol{I}_g^{\text{ini}} = \omega_0 k_{\text{pg}} \left(\boldsymbol{I}_g^{\text{ref}} - \boldsymbol{I}_g^{\text{ini}} \right)/L_g
\end{cases}
\tag{17}
$$

As can be seen from (13), (14), (16), (17), the dynamics of the RSC and GSC currents are decided by their initial states, current references, and PI control coefficients. Based on the analytical current expression, the parameters of the PI control can be selected to realize fast stabilization of the RSC and GSC current while avoiding overvoltage of converters caused by rapid change of the converter current.

Based on the analytical expressions of the stator, RSC and GSC current, their voltage can be separately calculated with the voltage equations, i.e., (2), (8) and (10) respectively.

III. OPTIMIZATION TO SDBR RESISTANCE UNDER UNCERTAIN FAULT SCENARIOS

A. OPTIMIZATION TARGET FOR SDBR

To select the SDBR resistance within its feasible range for the optimal LVRT effect, LVRT effect index with the SDBR is established combining the following two aspects:

(i) Capability to provide active power support

During the LVRT, SDBR may increase the stator voltage and avoid over speed of the rotor caused by the limited active power output of the stator. However, the SDBR absorbs most of the increased active power, thus it does not contribute to the active power support to the integrated grid. Instead, the larger SDBR resistance poses the stricter limit on the active current due to constraints of the stator voltage and the active power. The active power support capability of the DFIG is weakened.

The active power support capability is quantified by the difference of the active power output at the PCC during the LVRT compared with pre-fault operational state, as given by,

$$\Delta P = \int_0^{t_f} \mathrm{Re}\left[V_{PCC}^{ini}\left(I_g^{ini} - I_s^{ini}\right)^*\right] \\ -\mathrm{Re}\left[\sigma V_{PCC}^{ini}\left(I_g - I_s\right)^*\right] dt \quad (18)$$

where t_f denotes the fault duration.

(ii) Capability to damp electromagnetic torque oscillation

Once the SDBR is switched in, the electromagnetic torque of the DFIG will oscillate to a new steady state. The quick transition process is preferred to reduce the shaft oscillation and realize quick recovery from the fault. The real part of the damping coefficient τ in (5) increases with the larger SDBR resistance, i.e., the electromagnetic torque oscillation is better damped. Intensity of the electromagnetic torque oscillation is quantified by,

$$\Delta T_{em} = \int_0^{t_f} \left|L_m \mathrm{Im}\left(I_s I_r^*\right) - L_m \mathrm{Im}\left[I_s^\infty \left(I_r^\infty\right)^*\right]\right| dt \quad (19)$$

where T_{em} denotes the electromagnetic torque of the DFIG.

Since the increased SDBR resistance reduces the active power support capability of the DFIG and improves damping to the electromagnetic torque oscillation at the same time, a weighted sum of the indices in (18) and (19) is proposed to evaluate the LVRT effect with the SDBR,

$$A = W_1 \Delta P + W_2 \Delta T_{em} \quad (20)$$

where A is the LVRT effect index, W_1 and W_2 are the weight coefficients.

B. OPTIMIZATION MODEL FOR COORDINATED SDBR OPERATION AND CONVERTER CONTROL

For the SDBR resistance, ensuring the security of the DFIG during the LVRT process is the primary requirement, i.e., the current and voltage constraints of the stator, the RSC and the GSC.

To support the grid voltage, the reactive current injection [30] during the LVRT is a common requirement prescribed by grid codes [31]. The required reactive current

injection by the German grid code is given by,

$$\mathrm{Im}\left(I_s^\infty\right) - \mathrm{Im}\left(I_g^\infty\right) \geq 2\left(1 - \sigma\right) \quad (21)$$

As stated before, to achieve the optimal LVRT effect with the SDBR, coordination with the converter control is needed. With the given SDBR resistance and fault scenario, current references of the converter control are selected based on the LVRT effect index, and then applied to the RSC and GSC control as the SDBR switches in. The selection of the current reference is formulated as (22), where the security constraints and reactive current injection requirement is added.

$$\min A\left(I_r^{ref}, I_g^{ref}\right)$$
$$s.t. \; |V_s| \leq V_s^{max}, \; |V_r| \leq V_r^{max}, \; |V_g| \leq V_g^{max}$$
$$|I_s| \leq I_s^{max}, \; |I_r| \leq I_r^{max}, \; |I_g| \leq I_g^{max}$$
$$\mathrm{Im}\left(I_s^\infty\right) - \mathrm{Im}\left(I_g^\infty\right) \geq 2\left(1 - \sigma\right) \quad (22)$$

where superscript max denotes maximum allowable value.

The coordinated SDBR operation and converter control is illustrated in Fig. 3. When the SDBR switches in under the fault condition, the coordinated converter control is realized by assigning the current references that achieves the optimal LVRT effect. where V_{th} is the threshold voltage to trigger SDBR protection.
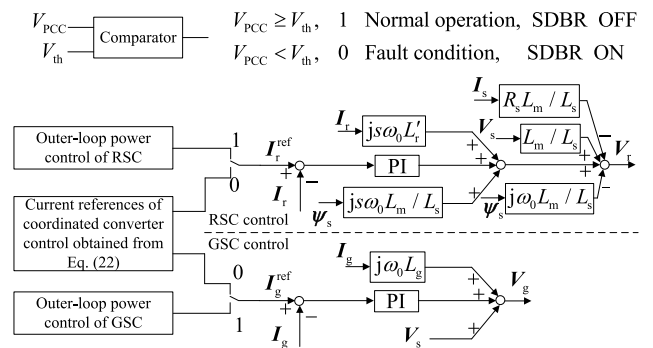
FIGURE 3. Coordinated SDBR operation and converter control.

C. SELECTION OF SDBR RESISTANCE AND SWITCH-IN CRITERION CONSIDERING FAULT UNCERTAINTIES

The LVRT effect of the DFIG varies under the different fault conditions with the same SDBR resistance. In this section, the uncertainties of the fault conditions are considered when optimizing the resistance of the SDBR.

(i) Impact of fault condition uncertainties on selection of SDBR resistance

As for the LVRT of the DFIG, the wind speed, the voltage drop depth, and the fault duration, are the mainly concerned fault conditions.

Under the low wind speeds, the maximum active power output of the DFIG is limited. In this case, the smaller SDBR resistance is preferred to reduce its active power consumption and improve the active power support capability of the DFIG.

For the deep voltage drops, the larger SDBR resistance can accelerate the damping of electromagnetic torque oscillation and better compensate for the stator voltage drop. The active power output deficiency of the DFIG is proportional to the fault duration while the index of the electromagnetic torque oscillation no longer varies with the fault duration once the torque reaches the steady state. The smaller SDBR resistance is preferred in the case of long fault durations for the better active power support capability of the DFIG.

(ii) Probabilistic modeling of fault condition uncertainties

The joint probability distribution including the wind speed, the voltage drop depth and the fault duration is given by [28],

$$Pr_{(v,\sigma,t_{\mathrm{f}})} = Pr_v Pr_{(\sigma,t_{\mathrm{f}})} \qquad (23)$$

where Pr denotes the probability distribution, v is the wind speed.

Assuming the probability distribution contains m discrete wind speed values, n discrete voltage drop depth values and l discrete fault duration values, the expectation of the LVRT effect index is given by,

$$E(A) = \sum_{x=1}^{m} \sum_{y=1}^{n} \sum_{z=1}^{l} Pr_{(v_x, \sigma_y, t_{fz})} A(v_x, \sigma_y, t_{fz}) \qquad (24)$$

where E denotes the expectation value.

Combining the probability distribution of fault conditions and the corresponding LVRT effect indices, overall LVRT effect of the DFIG is characterized by the expectation of the LVRT effect index.

(iii) Probabilistic optimal resistance and switch-in criterion of SDBR considering fault condition uncertainties

Normally the SDBR is switched in once the PCC voltage drops below 0.9 p.u. Given that the LVRT effect of the DFIG with the SDBR is influenced by the voltage drop depth, and the smaller SDBR resistance is preferred for minor voltage drops, it is difficult to select the SDBR resistance value that both has the desirable LVRT effect for the minor and deep voltage drops. However, with the properly reduced switch-in criterion for the SDBR, the larger SDBR resistance may be selected to deal with the deep voltage drops while the SDBR is not activated with minor voltage drops to avoid limitations on the active current output. Under the premise of adhering to the security constraints, modified switch-in criterion V_{th} is selected together with the SDBR resistance, and the value with the minimum expectation of the LVRT effect index is selected to achieve the optimal overall LVRT effect with all enumerated fault conditions.

Flow chart of the procedure to obtain optimal resistance value and switch-in criterion of the SDBR is given by Fig. 4.

IV. NUMERICAL ANALYSIS

Parameters of the test system shown in Fig. 1 are as follows. The air density is 1.225 kg/m^3 and the radius of wind turbine is 32.13 m. The C_{p} function is given by [32]. To evaluate the LVRT effect with simulation analysis, the DFIG is modelled based on the parameters from [33].
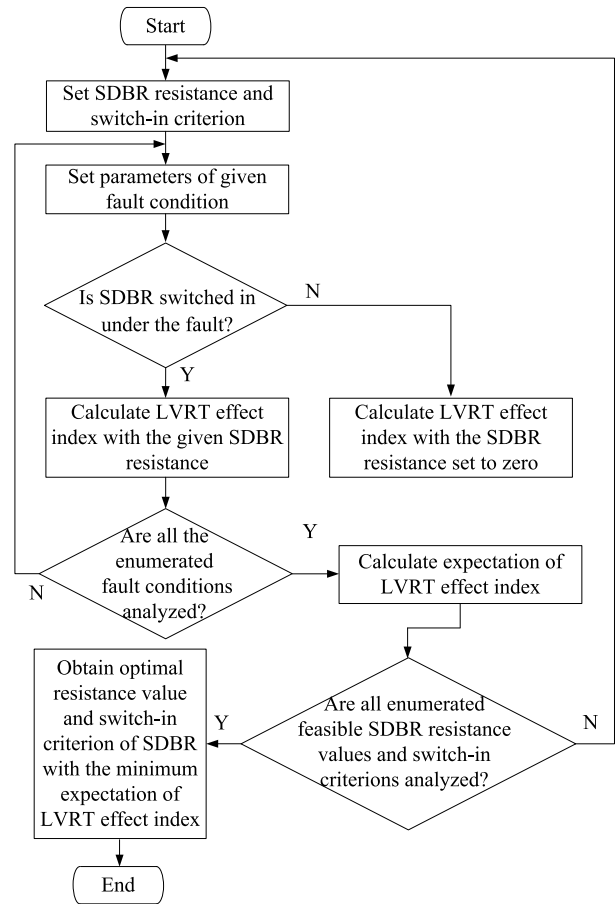

FIGURE 4. Flow chart of procedure to obtain optimal resistance value and switch-in criterion of SDBR.

Rated output and voltage of the DFIG are 1.5 MW and 690 V. L_{s}=3.07 p.u., L_{r}=3.056 p.u., L_{m}=2.9 p.u., R_{s}=0.00706 p.u., R_{r}=0.005 p.u., R_{g}=0.02 p.u., L_{g}=0.1 p.u., R_{ST}=0.02 p.u., L_{ST}=0.08 p.u., k_{pr}=1, k_{ir}=0.1, k_{pg}=1, k_{ig}=0.1.

To optimize the SDBR resistance, the weight coefficients of the evaluation index are set as W_1=1/2, W_2=1/2. During the LVRT, the active power output of the DFIG is not allowed to exceed 1.5 times the initial value to avoid rapid decrease of the rotor speed. Current and voltage constraints of the stator, RSC and GSC are $|I_{\mathrm{s}}|\leq 2$ p.u., $|V_{\mathrm{s}}|\leq 1.05$ p.u., $|I_{\mathrm{r}}|\leq 1.6$ p.u., $|V_{\mathrm{r}}|\leq 1.15$ p.u., $|I_{\mathrm{g}}|\leq 0.5$ p.u., $|V_{\mathrm{g}}|\leq 1.15$ p.u. [34], [35].

A. IMPROVED LVRT EFFECTS WITH MODIFIED REFERENCE FRAME FOR CONVERTER CONTROL

In this section, the improved LVRT effect with the modified reference frame for converter control is verified. Parameters of the LVRT scenario are as follows. The wind speed is v=10 m/s. The PCC voltage drops from 1 p.u. to 0.4 p.u. at t=0.05 s with the duration t_{f}=0.3 s. The SDBR resistance is R_{SDBR} = 0.1 p.u. The desired power output of the stator and the GSC are 0.6+j0.2 p.u. and 0.05+j0.25 p.u. respectively. Based on (7), corresponding current references of the RSC and GSC are $I_{\mathrm{r}}^{\mathrm{ref}}$=1.07−j0.57 p.u. and $I_{\mathrm{g}}^{\mathrm{ref}}$=0.08−j0.42 p.u.
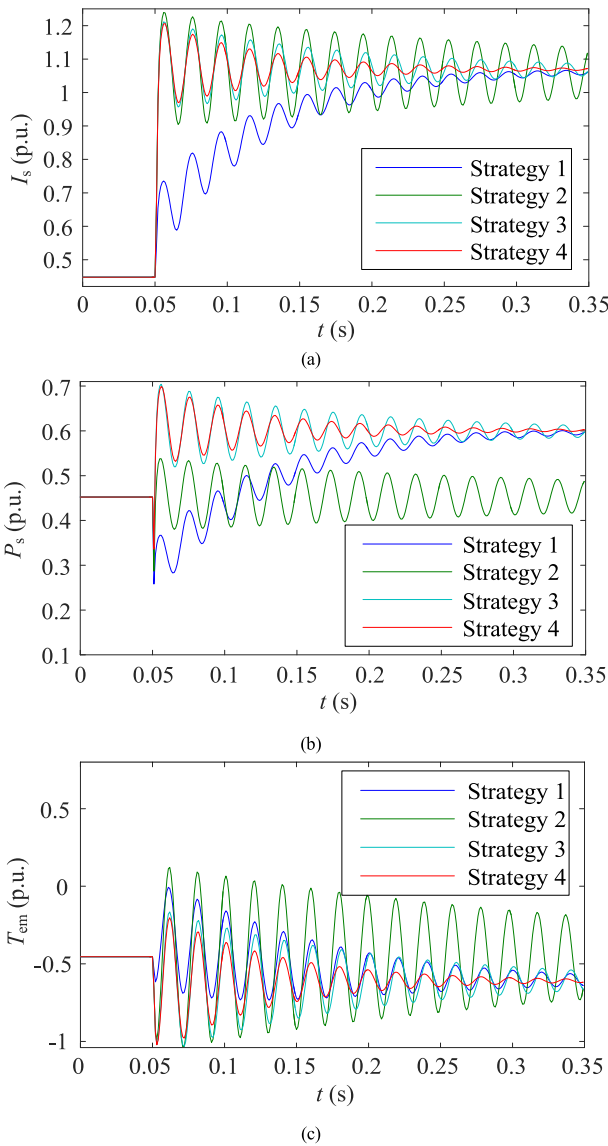
FIGURE 5. Comparison of LVRT effects with different control strategies of converters. (a) stator current. (b) stator active power. (c) electromagnetic torque.

To verify the improved control effect with modification to the reference frame, comparison of the LVRT effects is shown in Fig. 5.

Strategy 1: Apply SDBR & the dual-loop converter control with outer power loop.

Strategy 2: Apply direct converter current control only.

Strategy 3: Apply SDBR & direct converter current control in the traditional dq frame.

Strategy 4: Apply SDBR & direct converter current control in the xy frame of the PCC.

With strategy 1, due to the slow response of outer power loop, it takes much more time for the active power of the stator to reach its reference (seen from Fig. 5b). This shows that the direct converter current control helps to regulate the output power of the converter with the higher efficiency. As seen from Figs. 5a and 5c, improvement to the LVRT effect by the

SDBR is shown by the reduced oscillation of the stator current and the electromagnetic torque (strategy 3 vs strategy 2). To achieve the optimal LVRT effect with the combination of the converter current control and the SDBR, comparison between strategy 3 and strategy 4 shows that, by applying the xy frame of the PCC to converter control as a substitution of the traditional dq frame, the effect of the converter control is improved by avoiding the oscillation of the reference frame (seen from Fig. 5a), and electromagnetic torque oscillation is suppressed at the same time (seen from Fig. 5c).

B. VALIDATION TO ANALYTICAL EXPRESSION OF FAULT CURRENT

In this section, the accuracy of the analytical analysis on the LVRT transient is verified by comparing to the time-domain simulation results. Parameters of the LVRT scenario are as follows. The wind speed is $\upsilon = 10$ m/s. The PCC voltage drops from 1 p.u. to 0 p.u. at $t = 0.05$ s with the duration $t_\text{f} = 0.3$ s. The current references of the converter control are the same as those in Section A. The SDBR resistance is $R_\text{SDBR} = 0.1$ p.u. The comparison of the stator current, the RSC voltage and the electromagnetic torque between the analytical expression and the dynamic simulation is shown in Fig. 6.

The lines in Fig. 6 denoted as "analytical expression" are results obtained by directly calculating with the analytical expressions. As for the dynamic simulations, they rely on the numerical solution algorithms to simulate the LVRT transient by solving the differential and algebra equations of the DFIG model, e.g., the flux and voltage equation of DFIG (1). The analytical model and dynamic simulation are two different ways to evaluate the LVRT effect, thus accurate analytical expressions are supposed to be consistent with the dynamic simulation results. When deriving the analytical expressions, some assumptions are made, e.g., fast response of converter current control. The comparison in Fig. 6 is made to verify the accuracy of the derived analytical expressions.

The analytical expressions accord well with the dynamic simulation results, showing that the analytical expressions are capable to quantify the LVRT transient with the satisfactory accuracy. Thus, it can be used to formulate the optimization model to coordinate the converter control with the SDBR and select the optimal SDBR resistance value based on quantitive index of LVRT performance.

Fig. 6 also shows that, with the combination of the SDBR and the direct converter current control, the stator current and the RSC voltage of the DFIG are limited within the region of the security constraints. Thus, the adopted scheme is capable to meet the zero-voltage ride-through requirement by most of the grid codes.

Although both the derived analytical expressions and the dynamic simulation may be applied to evaluate the LVRT effect, the former shows some advantages over the latter in the optimization to the SDBR resistance. With the analytical expressions, how the SDBR affects the LVRT transient of the DFIG is quantified, e.g., in (5), the improved damping to the stator flux oscillation is revealed by the term R_SDBR/L_s in
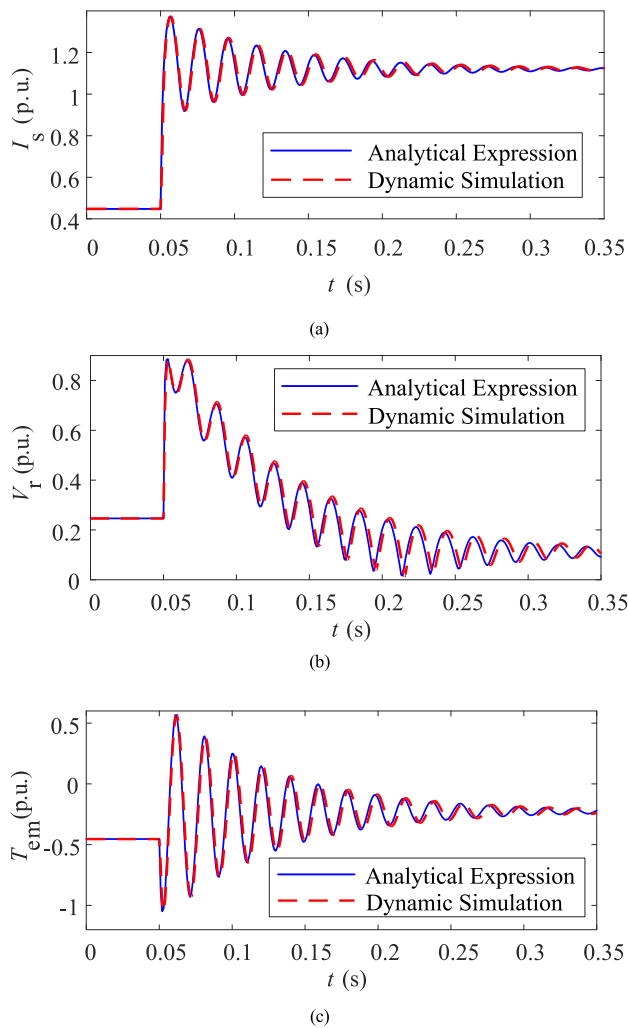
FIGURE 6. Comparison between analytical expression and dynamic simulation. (a) stator current. (b) RSC voltage. (c) electromagnetic torque.

the damping time constant τ. Also, optimization to the SDBR resistance involves calculation of the LVRT evaluation index. The calculation burden is reduced with the derived analytical expressions, as the numerical solution algorithm adopted by the dynamic simulation normally requires multiple iterations to solve the operation condition of the DFIG in each time interval of the simulation step. With the reduced calculation burden, less time is required for the program to obtain the optimization results. In Table 1, the time consumption of the analytical expression and the dynamic simulation to analyze single LVRT scenario is compared. Programs are run on the platform of MATLAB R2018b with the i5-7300HQ CPU, 2.5 GHz, 8 GB RAM PC. Improved calculation efficiency with the analytical expression is revealed by the comparison results shown in Table 1.

C. COORDINATION BETWEEN SDBR AND CURRENT CONTROL OF CONVERTERS

The performance of the SDBR to assist the LVRT is affected by the simultaneously applied converter control. To optimize

TABLE 1. Time consumption of single LVRT scenario analysis.

	Analytical expression	Dynamic simulation
Time consumption of single LVRT scenario analysis	0.0372 s	0.2074 s

the SDBR resistance based on its LVRT effect, coordination with the converter control needs to be considered in advance. When optimizing the SDBR resistance, the current references of the RSC and GSC for each feasible SDBR resistance are firstly selected to guarantee that the optimal LVRT effect, i.e., minimum LVRT effect index A in (22), is achieved for each feasible SDBR resistance with coordinated converter control. Then the different SDBR resistances are compared to select the optimal value with the superior LVRT effect.

With PCC voltage dropping to 0.4 p.u. from 0.05 s to 0.35 s, $I_r^{ref}=1.05+j0.61$ p.u. and $I_g^{ref}=0.42+j0.27$ p.u. are selected for $R_{SDBR}=0.1$ p.u. The electromagnetic torque of the DFIG and the active current of the PCC during the fault with different converter control schemes are compared in Fig. 7. Current references for scheme 1 are $I_r^{ref}=0.85+j0.41$ p.u. and $I_g^{ref}=0.17+j0.47$ p.u. Scheme 2 adopts the selected current references. And the current references for scheme 3 are $I_r^{ref}=1.25+j0.81$ p.u. and $I_g^{ref}=0.15+j0.2$ p.u.

With the selected current reference (scheme 2), the slighter electromagnetic torque oscillation is observed compared with scheme 3 (Fig. 7a) and the maximum active current output is realized among the three schemes (Fig. 7b), showing that the selected current reference achieves the optimal LVRT effect as it is selected based on the minimum LVRT effect index. It shows that even the same SDBR resistance provides varied LVRT effects with different current references of converter control. By selecting the current references of the RSC and GSC in the first place, the optimal LVRT effect of the SDBR is achieved by coordination with the converter current control.

D. IMPACT OF WIND SPEED ON LVRT EFFECT WITH COORDINATED SDBR AND CONVERTER CONTROL

As for the LVRT, the wind speed affects the initial operation state of the DFIG. Under the maximum power point tracking (MPPT) mode, the rotor speed of the DFIG transits from sub-synchronous speed to super-synchronous speed as the wind speed rises. In this section, the optimal LVRT effects of the DFIG that rotates respectively at the sub-synchronous speed and the super-synchronous speed are compared and analyzed. The following two scenarios are adopted:

Scenario 1: The wind speed is 7.3 m/s, the rotor speed of the DFIG is 0.85 p.u. (sub-synchronous speed)

Scenario 2: The wind speed is 9.8 m/s, the rotor speed of the DFIG is 1.15 p.u. (super-synchronous speed)

The PCC voltage drops from 1 p.u. to 0.6 p.u. at $t=0.05$ s with the duration $t_f=0.3$ s. The SDBR resistance is $R_{SDBR}=0.05$ p.u. The current references of the converter control are coordinated with the SDBR for the optimal LVRT effect.
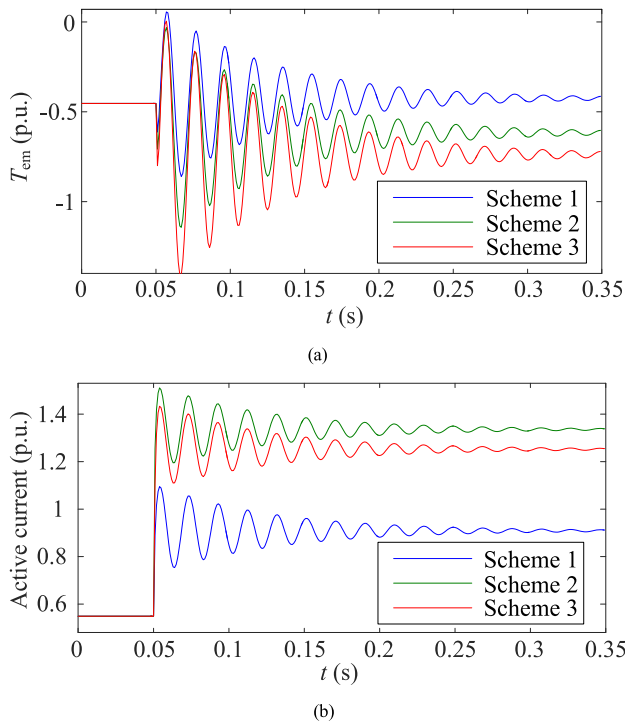
FIGURE 7. Comparison of LVRT effect with different current references.
(a) electromagnetic torque. (b) active current of PCC.

Comparison of electromagnetic torque, active and reactive current output of DFIG, and active power output of the GSC under scenario 1 and scenario 2 is shown in Fig. 8.

Under both scenarios, desirable LVRT effect is achieved with the SDBR and coordinated converter control. As seen from Fig. 8a, the required reactive current injection (0.8 p.u. under 40% voltage drop) is provided to the integrated grid by converter control. With the high wind speed (scenario 2), the capability of the DFIG to provide active power support is less constrained by the active power output limit, thus the larger active current is injected to the grid (seen from Fig. 8b). The increased active power output is accompanied by oscillation of the electromagnetic torque with the larger amplitude (seen from Fig. 8c).

Another difference in the operation of the DFIG between the sub-synchronous speed and the super-synchronous speed is the direction of the active power output of the GSC. When the DFIG rotates at the sub-synchronous speed at the initial of the LVRT, active power of the GSC transits from flowing to the DC bus to flowing to grid the during LVRT process. As seen from Fig. 8d, the larger variation of the GSC active power is observed with the sub-synchronous speed (scenario 1), which puts more stress on the protection of the DC bus as voltage deviation occurs with the imbalanced active power between the RSC and the GSC.

E. IMPACT OF DIFFERENT FAULT SCENARIOS ON OPTIMIZATION OF SDBR RESISTANCE

The LVRT effect of the DFIG with the SDBR is affected by the fault conditions, e.g., the wind speed, the voltage drop
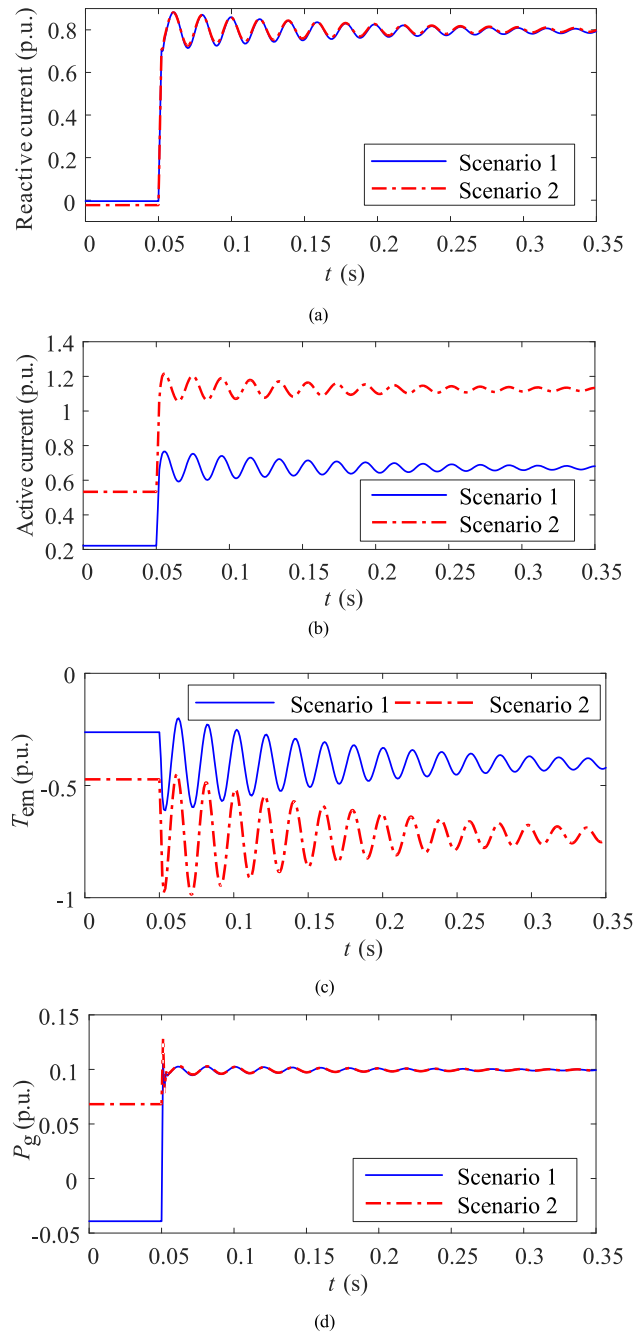

FIGURE 8. Comparison of LVRT effects under different wind speeds.
(a) reactive current output of DFIG. (b) active current output of DFIG.
(c) electromagnetic torque. (d) Active power output of GSC.

depth and the fault duration, which influence the selection of the SDBR resistance. The PCC voltage dropping to 0.2 p.u. for 0.2 s with the wind speed $\upsilon=10$ m/s is selected as the base case for the comparison of LVRT effects under different fault conditions. In Fig. 9, the minimum active power deficiency index ΔP and electromagnetic torque oscillation index ΔT_{em} with the SDBR under different fault conditions are compared.

With the increasing SDBR resistance, the minimum active power deficiency will increase remarkably once the SDBR resistance is large enough to trigger constraints of the stator
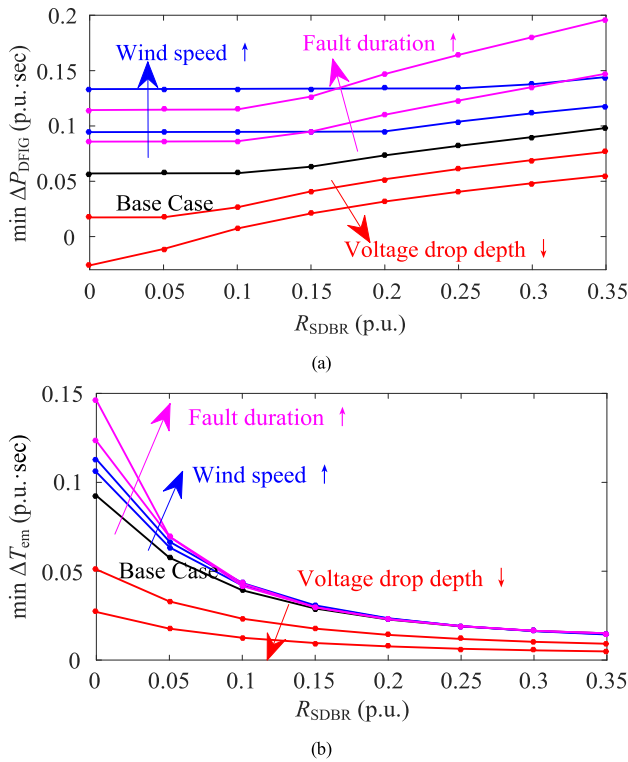
FIGURE 9. Comparison of LVRT effects under different fault conditions. (a) minimum active power deficiency. (b) minimum electromagnetic torque oscillation.

FIGURE 10. LVRT effect index under different fault conditions.

TABLE 2. Probability distribution of wind speed.

v	7	8	9	10	11	12	13
Pr_v	0.13	0.14	0.15	0.18	0.15	0.13	0.12

voltage and active power output, and consequently limit the output active current (Fig. 9a). This effect is relieved under higher wind speeds due to the larger active power constraints. Also, under the deeper voltage drops, with the smaller stator voltage, the critical SDBR resistance that triggers the stator voltage constraint is larger. Since the active power deficiency is proportional to the fault duration, this index goes up as the fault duration increases. To sum up, under fault conditions with low wind speeds, minor voltage drops, and long fault durations, the small SDBR resistance is preferred to improve the active power support capability of the DFIG.

Meanwhile, minimum electromagnetic torque oscillation reduces as the SDBR resistance increases, only with different marginal effects as shown in Fig. 9b. The improved damping to the electromagnetic torque oscillation is most significant in the cases of large voltage drop depth, since the stator voltage drop is the primary cause of the electromagnetic oscillation, and the SDBR helps to accelerate its damping. Besides, in all cases, marginal effect of the SDBR in oscillation damping become less remarkable as resistance value increases.

The minimum electromagnetic torque oscillation index and the minimum active power deficiency index separately quantifies the positive and negative effects of the increased SDBR resistance on the LVRT of the DFIG. The weighted sum of the indices as given by (20) is adopted to find the SDBR resistance with the optimal LVRT effect on the whole. The LVRT effect index under different fault conditions is shown in Fig. 10.
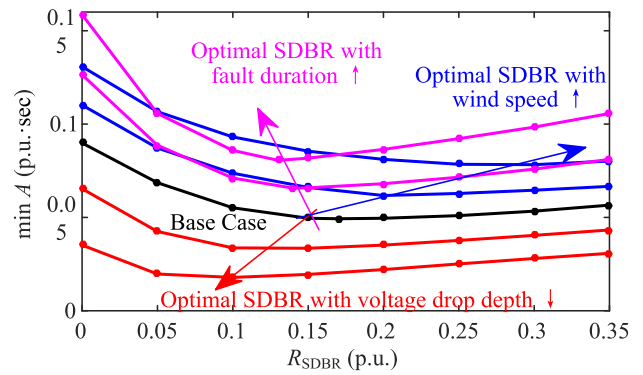
As can be seen from Fig. 10, for the higher wind speeds, output current of the DFIG is less constrained by the SDBR resistance with the better active power output capability, thus the larger SDBR resistance is selected to improve damping of the electromagnetic torque oscillation. For the minor voltage drops, as the SDBR resistance increases, the marginal effect of suppressing the electromagnetic oscillation becomes less remarkable. Meanwhile, the maximum active current output is reduced due to the stator voltage constraint, thus a smaller SDBR resistance is preferred to improve the active power support capability. The minimum active power deficiency is approximately proportional to the fault duration while the electromagnetic torque oscillation is no longer affected by the fault duration once the DFIG reaches the steady state, thus for the longer fault durations, a smaller SDBR resistance is selected to improve the active power support capability. To optimize the SDBR resistance, the influence of different fault scenarios on the LVRT performance needs to be evaluated. The selected SDBR resistance should be capable to achieve the optimal overall LVRT effect when considering multiple fault scenarios.

F. OPTIMIZATION TO SDBR RESISTANCE AND SWITCH-IN CRITERION WITH VARIOUS FAULT SCENARIOS

In this section, the SDBR resistance is optimized considering the uncertainties of the fault scenarios, which are described with the probability distribution. The probability distribution of the wind speed, voltage drop depth and fault duration are given in Table 2 and Table 3 respectively.

Based on the probability distribution of the fault conditions, expectation of the LVRT effect index with different switch-in criterions of the SDBR is shown in Fig. 11.

As seen from Fig. 11, for the traditional switch-in criterion of the SDBR ($V_{th} = 0.9$ p.u.), the 0.09 p.u. SDBR resistance achieves optimal overall LVRT effect for both the low wind

TABLE 3. Joint probability distribution of voltage drop depth and fault duration.

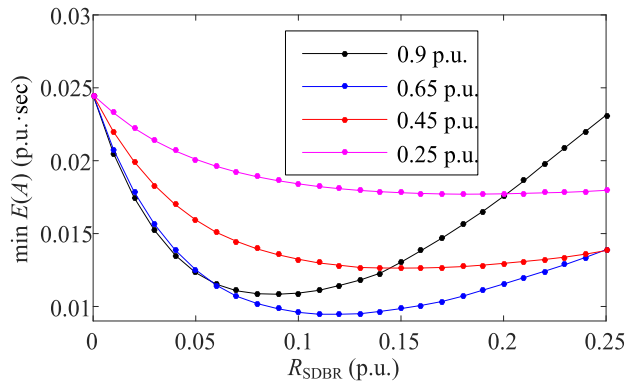| t_f \ σ	0.8	0.7	0.6	0.5	0.4	0.3	0.2
0.1	0.015	0.004	0.031	0.055	0.004	0.052	0.050
0.2	0.038	0.013	0.057	0.015	0.023	0.010	0.033
0.3	0.040	0.053	0.004	0.045	0.015	0.015	0.032
0.4	0.043	0.008	0.025	0.047	0.046	0.008	0.008
0.5	0.026	0.048	0.006	0.050	0.025	0.007	0.049

FIGURE 11. Expectation of LVRT effect index with different switch-in criterions of SDBR.

speed, minor voltage drop, long fault duration cases where the smaller SDBR resistance is preferred, and the high wind speed, deep voltage drop, short fault duration cases where the larger SDBR resistance is preferred.

The switch-in criterion is selected together with the SDBR resistance to achieve the optimal LVRT effect, i.e., minimum expectation of the LVRT effect index. With the modified voltage criterion ($V_{th} = 0.65$ p.u.), a larger SDBR resistance (0.11 p.u.) is selected to improve damping of electromagnetic torque oscillation under the deep voltage drops. While the SDBR is not switched in under minor voltage drops where the SDBR resistance might limit the active power support capability of the DFIG. It can be seen from Fig. 11 that the modified switch-in criterion achieves superior overall LVRT effect compared with the traditional scheme.

V. CONCLUSION

With the terminal-connected SDBR to assist the LVRT of the DFIG, the converter current control in the xy frame of the PCC is applied and coordinated with the SDBR to improve the LVRT effect. By deriving the analytical expression of the LVRT transient, a quantitive index to describe LVRT effect is established, which considers both the active power support capability of the DFIG and damping to the electromagnetic torque oscillation. Based on the probability distribution of the fault conditions, expectation of the LVRT index is adopted to optimize the SDBR resistance and the switch-in criterion for the optimal overall LVRT effect.

Some conclusions are yielded:

(i) Applying the converter current control in the xy frame of the PCC helps to avoid oscillation of the reference frame

resulted from the changing phase angle of the stator voltage, and the improved LVRT effect is realized compared with the converter current control in the traditional dq frame.

(ii) The derived analytical model of the LVRT process has the desirable accuracy compared with dynamic simulations, which can be used to formulate optimization model to select the SDBR resistance value with the optimal LVRT effect.

(iii) For the fault conditions with low wind speeds, minor voltage drops and long fault durations, smaller resistance of the SDBR is preferred to improve the active power output capability of the DFIG during the LVRT.

(iv) For the fault conditions with high wind speeds, deep voltage drops and short fault durations, larger resistance of the SDBR is preferred to better compensate for the stator voltage drop and improve damping to electromagnetic torque oscillation.

(v) With the reduced switch-in criterion, the larger SDBR resistance is selected to suppress the electromagnetic torque oscillation under the deep voltage drops, while the SDBR is not switched in for the minor voltage drops where the SDBR resistance might limit the active power support capability of the DFIG. The reduced switch-in criterion may improve the overall LVRT effect of the DFIG compared with traditional scheme.

REFERENCES

[1] S. Sang, C. Zhang, X. Cai, M. Molinas, J. Zhang, and F. Rao, "Control of a type-IV wind turbine with the capability of robust grid-synchronization and inertial response for weak grid stable operation," *IEEE Access*, vol. 7, pp. 58553–58569, 2019.

[2] D. Yang, Z. Jin, T. Zheng, and E. Jin, "An adaptive droop control strategy with smooth rotor speed recovery capability for type III wind turbine generators," *Int. J. Electr. Power Energy Syst.*, vol. 135, Feb. 2022, Art. no. 107532.

[3] S. Sang, N. Gao, X. Cai, and R. Li, "A novel power-voltage control strategy for the grid-tied inverter to raise the rated power injection level in a weak grid," *IEEE J. Emerg. Sel. Topics Power Electron.*, vol. 6, no. 1, pp. 219–232, Mar. 2018.

[4] C. Kim and W. Kim, "Enhanced low-voltage ride-through coordinated control for PMSG wind turbines and energy storage systems considering pitch and inertia response," *IEEE Access*, vol. 8, pp. 212557–212567, 2020.

[5] D. Yang, J. Kim, Y. C. Kang, E. Muljadi, N. Zhang, J. Hong, S.-H. Song, and T. Zheng, "Temporary frequency support of a DFIG for high wind power penetration," *IEEE Trans. Power Syst.*, vol. 33, no. 3, pp. 3428–3437, May 2018.

[6] A. M. S. Yunus, A. Abu-Siada, M. A. S. Masoum, M. F. El-Naggar, and J. X. Jin, "Enhancement of DFIG LVRT capability during extreme short-wind gust events using SMES technology," *IEEE Access*, vol. 8, pp. 47264–47271, 2020.

[7] K. E. Okedu, S. M. Muyeen, R. Takahashi, and J. Tamura, "Effectiveness of current-controlled voltage source converter excited doubly fed induction generator for wind farm stabilization," *Electr. Power Compon. Syst.*, vol. 40, no. 5, pp. 556–574, Mar. 2012.

[8] M. Rahimi and M. Parniani, "Efficient control scheme of wind turbines with doubly fed induction generators for low-voltage ride-through capability enhancement," *IET Renew. Power Gener.*, vol. 4, no. 3, pp. 242–252, May 2010.

[9] K. E. Okedu, "Enhancing DFIG wind turbine during three-phase fault using parallel interleaved converters and dynamic resistor," *IET Renew. Power Gener.*, vol. 10, no. 8, pp. 1211–1219, Sep. 2016.

[10] K. E. Okedu, S. M. Muyeen, R. Takahashi, and J. Tamura, "Wind farms fault ride through using DFIG with new protection scheme," *IEEE Trans. Sustain. Energy*, vol. 3, no. 2, pp. 242–254, Apr. 2012.

[11] H. Soliman, H. Wang, D. Zhou, F. Blaabjerg, and M. I. Marie, "Sizing of the series dynamic breaking resistor in a doubly fed induction generator wind turbine," in *Proc. IEEE Energy Convers. Congr. Expo. (ECCE)*, Sep. 2014, pp. 1–5.

[12] J. Mohammadi, S. Afsharnia, and S. Vaez-Zadeh, "Efficient fault-ride-through control strategy of DFIG-based wind turbines during the grid faults," *Energy Convers. Manage.*, vol. 78, pp. 88–95, Feb. 2014.

[13] J. Yang, J. E. Fletcher, and J. O'Reily, "A series-dynamic-resistor-based converter protection scheme for doubly-fed induction generator during various fault conditions," *IEEE Trans. Energy Convers.*, vol. 25, no. 2, pp. 422–432, Jun. 2010.

[14] M. Rahimi and M. Parniani, "Coordinated control approaches for low-voltage ride-through enhancement in wind turbines with doubly fed induction generators," *IEEE Trans. Energy Convers.*, vol. 25, no. 3, pp. 873–883, Sep. 2010.

[15] S. Tohidi, H. Oraee, M. R. Zolghadri, and P. J. Tavner, "Influence of different series dynamic resistors on low-voltage ride-through of brushless doubly fed induction generator," *Electr. Power Compon. Syst.*, vol. 43, nos. 8–10, pp. 995–1005, May 2015.

[16] W. Gao, G. Wang, and J. Ning, "Development of low voltage ride-through control strategy for wind power generation using real time digital simulator," in *Proc. IEEE/PES Power Syst. Conf. Expo.*, Mar. 2009, pp. 1–6.

[17] A. A. Hussein and M. H. Ali, "Comparison among series compensators for transient stability enhancement of doubly fed induction generator based variable speed wind turbines," *IET Renew. Power Gener.*, vol. 10, no. 1, pp. 116–126, Jan. 2016.

[18] M. Nasiri, J. Milimonfared, and S. H. Fathi, "A review of low-voltage ride-through enhancement methods for permanent magnet synchronous generator based wind turbines," *Renew. Sustain. Energy Rev.*, vol. 47, pp. 399–415, Jul. 2015.

[19] S. M. Muyeen, "A combined approach of using an SDBR and a STATCOM to enhance the stability of a wind farm," *IEEE Syst. J.*, vol. 9, no. 3, pp. 922–932, Sep. 2015.

[20] Z. Dao and F. Blaabjerg, "Optimized demagnetizing control of DFIG power converter for reduced thermal stress during symmetrical grid fault," *IEEE Trans. Power Electron.*, vol. 33, no. 12, pp. 10326–10340, Dec. 2018.

[21] S. Kihwele, "On control and operating strategies for maximizing the controllability of the DFIG wind turbine during grid disturbance," in *Proc. Int. Conf. Electron., Inf., Commun. (ICEIC)*, Jan. 2016, pp. 1–4.

[22] M. Asif, R. Bux, and R. A. Memon, "Improved RSC-GSC decoupled and LVRT control strategies of DFIG-based wind turbine," in *Proc. Int. Conf. Electr. Eng. (ICEE)*, Feb. 2018, pp. 1–4.

[23] J. Lopez, P. Sanchis, X. Roboam, and L. Marroyo, "Dynamic behavior of the doubly fed induction generator during three-phase voltage dips," *IEEE Trans. Energy Convers.*, vol. 22, no. 3, pp. 709–717, Sep. 2007.

[24] K. E. Okedu, S. M. Muyeen, R. Takahashi, and J. Tamura, "Application of SDBR with DFIG to augment wind farm fault ride through," in *Proc. Int. Conf. Electr. Mach. Syst.*, Aug. 2011, pp. 1–6.

[25] P.-H. Huang, M. S. El Moursi, W. Xiao, and J. L. Kirtley, Jr., "Novel fault ride-through configuration and transient management scheme for doubly fed induction generator," *IEEE Trans. Energy Convers.*, vol. 28, no. 1, pp. 86–94, Mar. 2013.

[26] X. Wu, A. Arulampalam, C. Zhan, and N. Jenkins, "Application of a static reactive power compensator (STATCOM) and a dynamic braking resistor (DBR) for the stability enhancement of a large wind farm," *Wind Eng.*, vol. 27, no. 2, pp. 93–106, Mar. 2003.

[27] M. Wang, Y. Tian, X. Feng, and G. Chen, "A hybrid LVRT control scheme for PMSG wind power system," in *Proc. 7th Int. Power Electron. Motion Control Conf.*, Jun. 2012, pp. 1173–1177.

[28] S. S. Smater and A. D. Dominguez-Garcia, "A framework for reliability and performance assessment of wind energy conversion systems," *IEEE Trans. Power Syst.*, vol. 26, no. 4, pp. 2235–2245, Nov. 2011.

[29] J.-B. Hu and Y.-K. He, "Dynamic modelling and robust current control of wind-turbine driven DFIG during external AC voltage dip," *J. Zhejiang Univ.-Sci. A*, vol. 7, no. 10, pp. 1757–1764, Oct. 2006.

[30] X. Chen, W. Wu, N. Gao, H. S.-H. Chung, M. Liserre, and F. Blaabjerg, "Finite control set model predictive control for LCL-filtered grid-tied inverter with minimum sensors," *IEEE Trans. Ind. Electron.*, vol. 67, no. 12, pp. 9980–9990, Dec. 2020.

[31] D. Xie, Z. Xu, L. Yang, J. Østergaard, Y. Xue, and K. Wong, "A comprehensive LVRT control strategy for DFIG wind turbines with enhanced reactive power support," *IEEE Trans. Power Syst.*, vol. 28, no. 3, pp. 3302–3310, Aug. 2013.

[32] S. Heier, *Grid Integration of Wind Energy Conversion Systems*. Chichester, U.K.: Wiley, 1998.

[33] R. Bhattarai, N. Gurung, S. Ghosh, and S. Kamalasadan, "Parametrically robust dynamic speed estimation based control for doubly fed induction generator," *IEEE Trans. Ind. Appl.*, vol. 54, no. 6, pp. 6529–6542, Nov. 2018.

[34] S. Xiao, H. Geng, H. Zhou, and G. Yang, "Analysis of the control limit for rotor-side converter of doubly fed induction generator-based wind energy conversion system under various voltage dips," *IET Renew. Power Gener.*, vol. 7, no. 1, pp. 71–81, Jan. 2013.

[35] S. Liu, T. Bi, K. Jia, and Q. Yang, "Coordinated fault-ride-through strategy for doubly-fed induction generators with enhanced reactive and active power support," *IET Renew. Power Gener.*, vol. 10, no. 2, pp. 203–211, Feb. 2016.

JIEJIE HUANG received the B.S. and Ph.D. degrees in electrical engineering from the Hefei University of Technology, Hefei, China, in 2015 and 2020, respectively.

He is currently a Lecturer with the School of Electrical Engineering, Nantong University, Nantong, China. His research interests include the stability and control of wind power systems.

LEI ZHANG (Member, IEEE) was born in Nantong, China, in 1992. He received the B.Eng. degree in electrical engineering and automation and the Ph.D. degree in electrical engineering from the China University of Mining and Technology, Xuzhou, China, in 2014 and 2019, respectively.

Since 2019, he has been with the School of Electrical Engineering, Nantong University, where he is currently a Lecturer. His current research interests include power electronics, application of SiC MOSFETs, and modeling and control of the renewable power generation.

SHUN SANG received the B.S. degree in electrical engineering from the China University of Mining and Technology, Xuzhou, China, in 2014, and the Ph.D. degree from the Wind Power Research Center, Shanghai Jiao Tong University, Shanghai, China, in 2020.

He was a Ph.D. Visiting Scholar with the Department of Engineering Cybernetics, Norwegian University of Science and Technology, Trondheim, Norway, in 2018. He is currently a Lecturer with the School of Electrical Engineering, Nantong University, Nantong, China. His research interests include the control of wind turbines, and interactive stability issues between wind power converters and ac grids.

XIAOCEN XUE received the B.S. degree in computer science and technology and the Ph.D. degree in power engineering and engineering thermal physics from Southeast University, Nanjing, China, in 2007 and 2015, respectively.

He is currently a Lecturer with the School of Electrical Engineering, Nantong University, Nantong, China. His research interests include electricity market and energy internet.

XINSONG ZHANG received the B.E. degree in electrical engineering from the Xi'an University of Technology, Xi'an, China, in 2002, the M.Sc. degree in electrical engineering from Xi'an Jiaotong University, Xi'an, in 2005, and the Ph.D. degree from Hohai University, Nanjing, China, in 2013.

He joined the Faculty of Nantong University, China, in 2006. From 2018 to 2019, he was an Academic Visitor with the Department of Electronic and Electrical Engineering, University of Bath, Bath, U.K. He is currently a Professor with the School of Electrical Engineering, Nantong University. His research interests include power systems operation and planning, wind power integration, and energy storage systems.

WEIMIN WU (Member, IEEE) received the Ph.D. degree in electrical engineering from the College of Electrical Engineering, Zhejiang University, Hangzhou, China, in 2005.

He worked as a Research Engineer with the Delta Power Electronic Center, Shanghai, China, from July, 2005 to June 2006. Since July 2006, he has been a Faculty Member with Shanghai Maritime University, where he is currently a Full Professor with the Department of Electrical Engineering. He was a Visiting Professor with the Center for Power Electronics Systems, Virginia Polytechnic Institute and State University, Blacksburg, VA, USA, from September 2008 to March 2009. From November 2011 to January 2014, he was a Visiting Professor with the Department of Energy Technology, Aalborg University, Aalborg, Demark, working at the Center of Reliable Power Electronics. He has coauthored more than 100 articles and holds eight patents. His research interests include power converters for renewable energy systems, power quality, smart grid, and energy storage technology.

Dr. Wu serves as an Associate Editor for the IEEE TRANSACTIONS ON INDUSTRY ELECTRONICS.

TINGTING SUN received the B.S. and M.S. degrees in electrical engineering from the Hefei University of Technology, Hefei, China, in 2016 and 2019, respectively.

She is currently a Teaching Assistant with the School of Electrical and Energy Engineering, Nantong Institute of Technology, Nantong, China. Her research interests include the integration of wind power generation through VSC-HVDC and frequency stability analysis.

NING GAO (Associate Member, IEEE) received the B.S. degree in electronics and information engineering from Zhejiang University, Hangzhou, China, in 2009, and the M.S. and Ph.D. degrees in electrical engineering from Shanghai Jiao Tong University, Shanghai, China, in 2011 and 2017, respectively. Since 2017, he has been with the Department of Electrical Engineering, Shanghai Maritime University, Shanghai, where he is currently an Associate Professor. His current research interest includes power converters applied in battery energy storage systems.

● ● ●